All-optical isolator under arbitrary linearly polarized fundamental wave in an optical superlattice

Liang Yuan,[1] Jianhong Shi,[1,2] and Xianfeng Chen[1,3]

[1]Department of Physics; The State Key Laboratory on Fiber Optic Local Area Communication Networks and
Advanced Optical Communication Systems, Shanghai Jiao Tong University,
800 Dongchuan Road, Shanghai 200240, China

[2]e-mail: purewater@sjtu.edu.cn

[3]e-mail: xfchen@sjtu.edu.cn

We theoretically investigate an all-optical isolator under arbitrary linearly polarized fundamental wave (FW) input in an optical superlattice (OSL). The scheme is based on simultaneously phase matching the first-order Type I (oo-e) quasi-phase-matching (QPM) second-harmonic generation (SHG) process and higher-order Type 0 (ee-e) QPM SHG process in an OSL with a defect inserted in an asymmetrical position. Simulation results show that the contrast ratio of the all-optical isolator can maintain close to 1 under arbitrary linearly polarized FW. Thus, an all-optical isolator based on an OSL that is not sensitive to the direction of linear polarization can be realized. We also show that, with the defect in a strong asymmetry position, the length of the defect can be designed flexibly to maintain a high contrast ratio. Additionally, if the length of the OSL is longer, the nonreciprocal response can be realized for low optical intensities.   © 2011 Optical Society of America

OCIS codes: 190.2620, 160.4330.

1. Introduction

The optical isolator as an indispensable element in fiber optical communication and semiconductor laser diode systems has attracted significant interest because it can reduce problems caused by unwanted reflections or interference effects. A standard magneto-optic Faraday rotator combined with polarizers compose the conventional optical isolator that is the most widely used. Based on the magnetic-optical effect, much effort has been expended in developing integrated magnetic isolators [1–3]. As demand keeps increasing for nonmagnetic optical isolators in integrated photonic systems, several schemes, including planar chiral metamaterials [4], negative-refraction metamaterials [5], or indirect photonic interband transitions [6], have been proposed. Recently, second-harmonic generation (SHG) in optical superlattices

(OSLs) has attracted much attention as a means of achieving a unidirectional and bidirectional tunable optical isolator [7–11]. This scheme relies on two principles. First, the phase-matching condition should be satisfied to guarantee an efficient SHG process. Second, the structure must be spatially asymmetric so that the fundamental wave (FW, ω) converts more strongly to the second-harmonic wave (SHW, 2ω) from one direction (e.g., from the backward direction) than from the other direction. Therefore, when combined with an absorption filter centered at 2ω, the FW will exhibit an optical isolator effect. The contrast ratio of the optical isolator is defined as $C = (T_\lambda^+ - T_\lambda^-)/(T_\lambda^+ + T_\lambda^-)$, where T_λ^+ and T_λ^- are the FW transmissions in the forward and backward directions, respectively. For those proposed optical diodes based on the SHG process, polarizers should be used to get a fixed polarization of the FW (typically z polarized in the case of lithium niobate, to maximize the effective nonlinearity), since the SHG processes are usually polarization dependent [7–11].

However, the polarizers will undoubtedly decay the initial energy of the FW and make the configuration more expensive. As is well known, the state of polarization is linearly polarized in semiconductor laser diode systems. Thus it is desired to develop a kind of all-optical isolator under arbitrary linearly polarized input light for semiconductor laser diode systems.

In this paper, we use a multi-phase-matching technique to realize all-optical isolator action under an arbitrary linearly polarized FW in an OSL. The multi-phase-matching technique includes cascaded [12], dual-periodic [13,14], and quasi-periodic [15,16] structures. Our scheme is based on simultaneous phase-matched first-order Type I (oo-e) and high-order Type 0 (ee-e) SHG in periodically poled lithium niobate (PPLN) with geometrical asymmetry. We present a phenomenon that the contrast ratio of the optical isolator can maintain close to 1 under an arbitrary linearly polarized FW. The all-optical isolator action influenced by the defect, the input FW intensity, and the length of the crystal are also discussed. All the results are based on the numerical calculation of the coupling wave equations among these waves.

2. Theoretical Analysis

Most quasi-phase-matching (QPM) processes in lithium niobate are designed to target the largest intrinsic nonlinear coefficient in lithium niobate, d_{33}. In terms of QPM SHG, we denote this the Type 0 process (zz-z), as the d_{33} coefficient couples z-polarized fundamentals to z-polarized harmonics [17,18]. Lithium niobate does, however, have an appreciable d_{31} coefficient, which can be used for a Type I process (yy-z), where y-polarized fundamentals couple to z-polarized harmonics. The Type I process can still be used as an attractive alternative for the SHG process and the SHG/difference-frequency-generation cascading process for its broadband wavelength acceptance [19,20]. According to the Sellmeier data of lithium niobate [21], first-order Type I and high-order Type 0 QPM SHG can be simultaneous phase
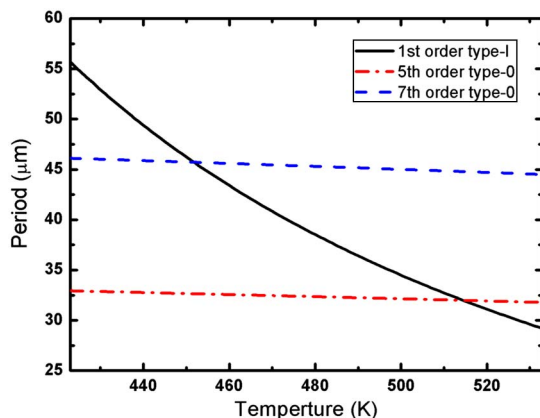

Fig. 1. (Color online) Required fabrication periods versus the temperature for phase-matched Type I (black solid curve), and fifth- (red dashed–dotted curve) and seventh- (blue dashed curve) order Type 0 QPM SHG at 1064 nm.

matched at appropriate temperatures and wavelengths. Figure 1 shows the required period for Type 0 and Type I QPM SHG for the wavelength of 1064 nm, as a function of the crystal temperature. We find two suitable periods in PPLN for simultaneous phase matching of two SHG processes: (a) the period $45.78\,\mu$m at $453.11\,$K to phase match the first-order Type I and seventh-order Type 0 SHG process, and (b) the period $31.99\,\mu$m at $515.15\,$K to phase match the first-order Type I and fifth-order Type 0 SHG process.

In this case, both the z-polarized and y-polarized FWs contribute to the SHG, so the coupling equations can be deduced as follows:

$$\frac{dA_{1y}(x)}{dx} = -i\sigma_1 A_{2z}A_{1y}^* \exp(-i\Delta k_1 x),$$
$$\frac{dA_{1z}(x)}{dx} = -i\sigma_2 A_{2z}A_{1z}^* \exp(-i\Delta k_0 x),$$
$$\frac{dA_{2z}(x)}{dx} = -i\sigma_1 A_{1y}A_{1y} \exp(i\Delta k_1 x)$$
$$\qquad\qquad - i\sigma_2 A_{1z}A_{1z} \exp(i\Delta k_0 x), \qquad (1)$$

with

$$A_{j\xi} = \sqrt{\frac{n_j}{\omega_j}} E_{j\xi},$$
$$\sigma_1 = \frac{g_2 d_{31}}{c}\sqrt{\frac{\omega_1^2 \omega_2}{n_{1z}^2 n_{2z}}},$$
$$\sigma_2 = \frac{g_2 d_{33}}{c}\sqrt{\frac{\omega_1^2 \omega_2}{n_{1z}^2 n_{2z}}},$$

where $E_{j\xi}$, ω_j, and $n_{j\xi}$ ($j = 1, 2$ referring to the FW and the SH, respectively, and $\xi = y, z$ representing the polarization orientation) are the electric fields, the angular frequencies, and the refractive indices, respectively. c is the speed of light in vacuum, and d_{33} and d_{31} are the nonlinear coefficients. As the structure function $f(x)$ is a periodic function of x with period Λ due to the periodically modulated nonlinear coefficient, it can be written as a Fourier series, $f(x) = \sum_m g_m \exp(-iG_m x)$, where G_m are the reciprocal vectors and g_m are the amplitudes of the reciprocal vectors. The QPM conditions for these processes is $\Delta k_1 = k_{2z} - 2k_{1z} - G_{m_1} = 0$ and $\Delta k_0 = k_{2z} - 2k_{1y} - G_{m_2} = 0$, where m_1 and m_2 are the orders of the QPM vector, $G_m = 2\pi m/\Lambda$.

3. Simulation Results

A schematic diagram of an all-optical isolator under an arbitrary linearly polarized FW input is shown in Fig. 2. In our simulation, the input intensity of the FW is 80 MW/cm^2, $L = 4$ cm, $d_{33} = 27$ pm/V, and $d_{31} = 4.7$ pm/V. The intensity ratio between the y-polarized components and the total input light, defined as P_y/P, whose value is from 0 to 1, represents
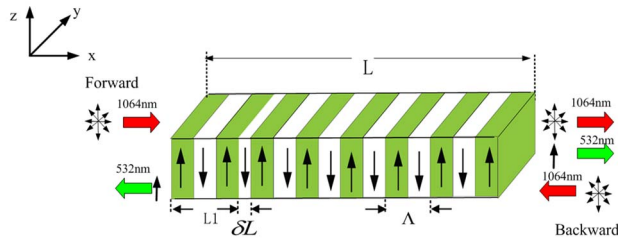
Fig. 2. (Color online) Schematic diagram of the all-optical isolator under arbitrary linearly polarized FW input. Λ is the period of grating. A defect is introduced at $x = L_1$ with a length δL.

the arbitrary linearly polarized light. A defect is introduced at a distance $L_1/L = 0.1$ from $x = 0$ with a length $\delta L = 0.2\Lambda$, which disturbs the coupling behavior of the SHG cascading process in forward and backward propagation by imposing dephasing between the FW and the SHW. The amount of dephasing determined by the length of the defect can be written as $\Delta\varphi = (2\delta L/\Lambda - 1)\pi$. Figure 3 shows the FW transmission in both direction and contrast ratio under arbitrary linearly polarized FW input. We should stress here that the FW transmission contains the transmission of both the y-polarized and z-polarized components. Thus a new contrast ratio can be defined as $C = (T_{1y}^+ + T_{1z}^+) - (T_{1y}^- + T_{1z}^-)/(T_{1y}^+ + T_{1z}^+) + (T_{1y}^- + T_{1z}^-)$. In Fig. 3(a), the period of the crystal is chosen to simultaneously phase match the first Type I and the seventh Type 0 SHG ($\Lambda = 45.78\,\mu$m). It is seen that the FW transmission in the forward direction is maintained at a relatively high value (40%–72%) under the random linearly polarized FW input, while the FW transmission in the backward direction is almost close to 0, although there exists some slight difference under the different polarization states of the FW. Therefore, the contrast ratio can be maintained close to 1, regardless of the direction of linear polarization. Figure 3(b) shows the scheme based on simultaneously phase-matched first Type I and fifth Type 0 SHG

($\Lambda = 31.99\,\mu$m). Under most of the linear polarization states, the contrast ratio is close to 1, except when the FW has few y-polarized components. In this sense, simultaneous phase-matched first Type I and seventh Type 0 SHG is more suitable for realizing a high-contrast all-optical isolator under an arbitrary linearly polarized FW. In addition, the temperature and period required are more convenient for both fabrication and operation (see Fig. 1). Thus, simultaneous phase-matched first-order Type I and seventh-order Type 0 SHG processes will be discussed in the following text.

To further investigate the principle of the all-optical action under an arbitrary linearly polarized FW, the detailed evolution of the FW and SHW coupling inside the crystal under any two linearly polarized FWs is shown in Fig. 4. Without loss of generality, $P_y/P = 0.2$ and $P_y/P = 0.8$ are selected in the simulation. Figures 4(a) and 4(b) show the coupling process in different directions under the FW polarization state of $P_y/P = 0.2$. In the forward direction, the FW propagates from the left to right. The intensity of the SHW improves rapidly due to the phase-matching condition. If there is no defect, the FW will completely convert to SHW. However, after the waves propagating through the defect, the introduced dephasing causes the energy to exchange alternately between the FW and the SHW, which results in 67.13% at the output in the transmission of the FW. In the backward direction, the FW propagates from the right to left. We see that the FW energy continuously transforms to the SHW and, consequently, the FW almost depletes to 0 when the waves propagate a certain length. Correspondingly, the coupling behavior under the FW polarization state of $P_y/P = 0.8$ is plotted in Figs. 4(c) and 4(d). It is interesting to find that the curves in Fig. 4(d) are similar to those of Fig. 4(b). That is because the long efficient interaction length allows the FW to almost convert to the SHW before reaching the defect, thus the FW transmission will approach
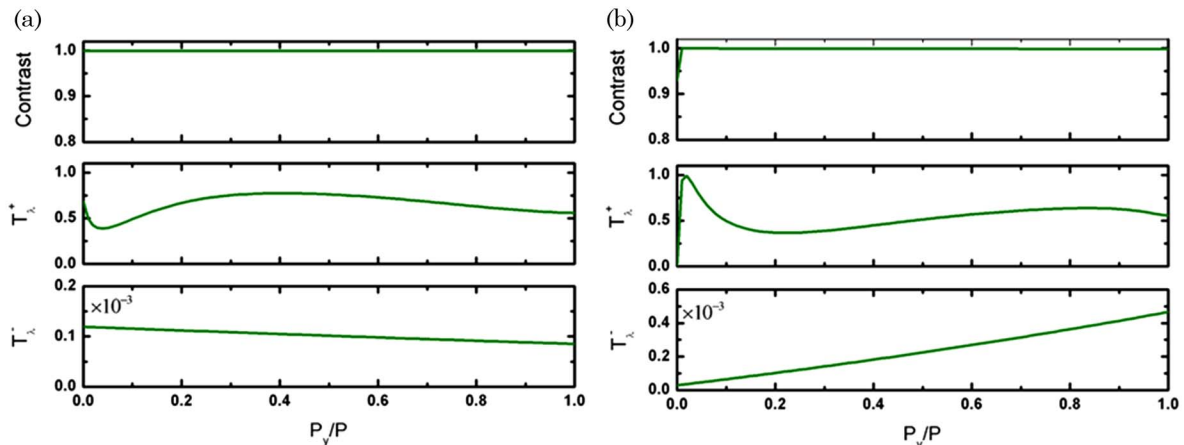

Fig. 3. (Color online) Transmission in both directions and the contrast ratio under an arbitrary linearly polarized FW based on (a) simultaneously phase-matched first-order Type I and seventh-order Type 0 SHG processes, and (b) simultaneously phase-matched first-order Type I and fifth-order Type 0 SHG processes.
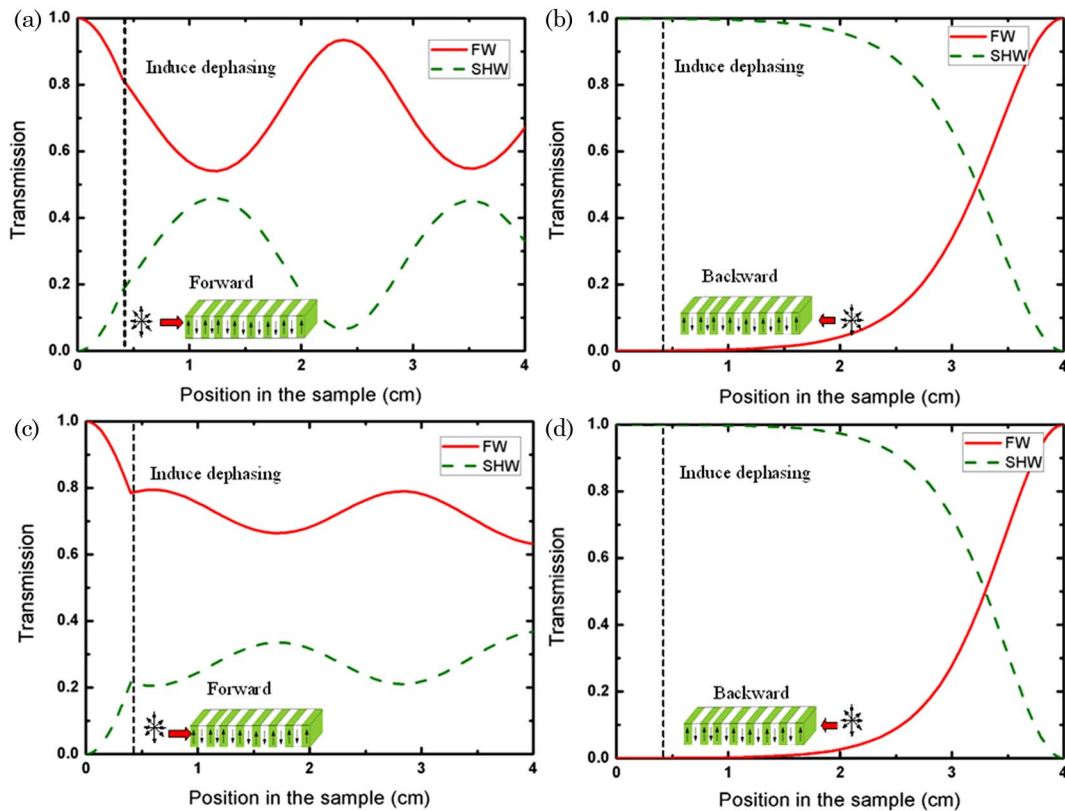
Fig. 4. (Color online) Evolution of two-wave coupling of the SHG processes inside the crystal under two different linearly polarized FW. (a) $P_y/P = 0.2$; the FW propagates from left to right. (b) $P_y/P = 0.2$; the FW propagates from right to left. (c) $P_y/P = 0.8$; the FW propagates from left to right. (d) $P_y/P = 0.8$; the FW propagates from right to left.

0 regardless of the phase contribution $\Delta\varphi$. So, however the polarization state of the FW changes, the transmission of the FW is always at a relatively high value in forward propagation but always close to 0 in backward propagation, thus the contrast maintains as 1 under arbitrary linearly polarized FW input.

Figure 5 shows that the contrast ratio is influenced by the position and length of the defect. The input

intensity and the length of the crystal are the same as in Fig. 3. Figure 5(a) describes the contrast ratio influenced by the position of the defect, and the length is fixed at $\delta L = 0.2\Lambda$. It is apparent that a high contrast ratio can be obtained under arbitrary linearly polarized FW for the strong asymmetry geometrical structure ($L_1/L = 0.1, 0.2, 0.25$). When $L_1/L = 0.3$, the contrast ratio declines as the P_y/P
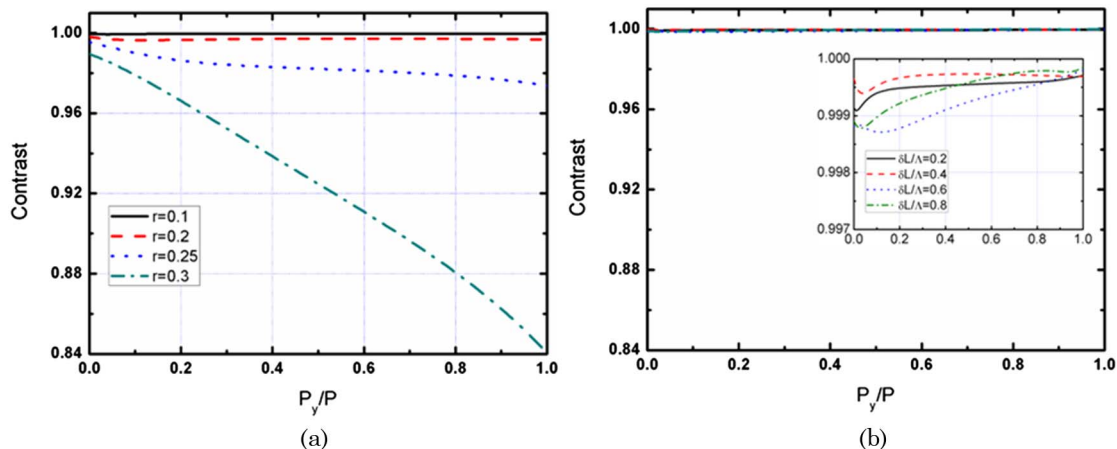

Fig. 5. (Color online) Contrast ratio influenced by the position and length of the defect under an arbitrary linearly polarized FW. (a) $\delta L = 0.4\Lambda$, $L_1/L = 0.1$ (black solid curve), 0.2 (red dashed curve), 0.25 (blue dotted curve), 0.3 (olive dashed–dotted curve). (b) $L_1/L = 0.1$, $\delta L = 0.2\Lambda$ (black solid curve), 0.4Λ (red dashed curve), 0.6Λ (blue dotted curve), 0.8Λ (olive dashed–dotted curve). The inset shows the details of (b).
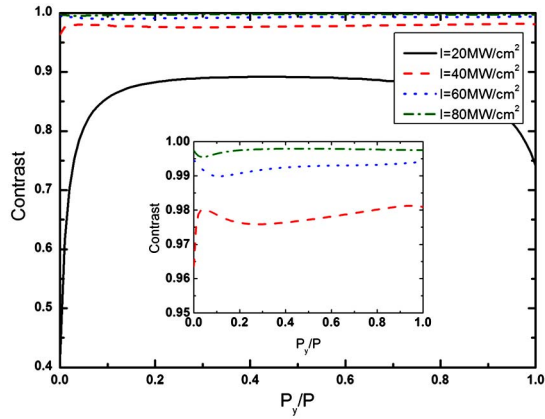
Fig. 6. (Color online) Contrast ratio influenced by the input FW intensity under an arbitrary linearly polarized FW while $L = 4\,\text{cm}$, $L_1/L = 0.1$, $\delta L = 0.2\Lambda$. The black solid, red dashed, blue dotted, and olive dashed–dotted curves correspond to $I = 20\,\text{MW/cm}^2$, $40\,\text{MW/cm}^2$, $60\,\text{MW/cm}^2$, and $80\,\text{MW/cm}^2$. The inset shows the details of the curves corresponding to $I = 40\,\text{MW/cm}^2$, $60\,\text{MW/cm}^2$, and $80\,\text{MW/cm}^2$.

increases. As a consequence, it is difficult to maintain a high contrast ratio under the arbitrary linear polarization state of the FW. The length of the defect also affects the contrast ratio, since it determines the amount of dephasing $\Delta\varphi$. It is different from other

reports that the length of defect or $\Delta\varphi$ plays an important role in the contrast [7,8]. In our proposed structure, the contrast ratio is insensitive to the length of the defect when the defect is in the strong asymmetry position of a relatively long crystal. In Fig. 5(b), the position of the defect is fixed at $L_1/L = 0.1$. It is found that nearly all the curves parallel to 1 when we choose different lengths of the defect, and the inset of Fig. 5(b) shows the details of the different curves. So in practical application, the defect should be introduced in the strong asymmetry position of the structure, which can offset the error of the design and fabrication processes to realize such all-optical isolator system.

The input FW intensity is another factor that also plays an important role in the contrast ratio. Different input FW intensities are assumed in our investigation for $L = 4\,\text{cm}$, $L_1/L = 0.1$, and $\delta L = 0.2\Lambda$. The simulation results are shown in Fig. 6. When $I = 20\,\text{MW/cm}^2$, the contrast ratio is lower than 0.9. The inset figure shows the details of the curves when $I = 40\,\text{MW/cm}^2$, $60\,\text{MW/cm}^2$, and $80\,\text{MW/cm}^2$, and increasing the input intensity can raise the contrast ratio close to 1.

However, high-intensity FW input would cause photorefractive damage in the ferroelectric crystal.
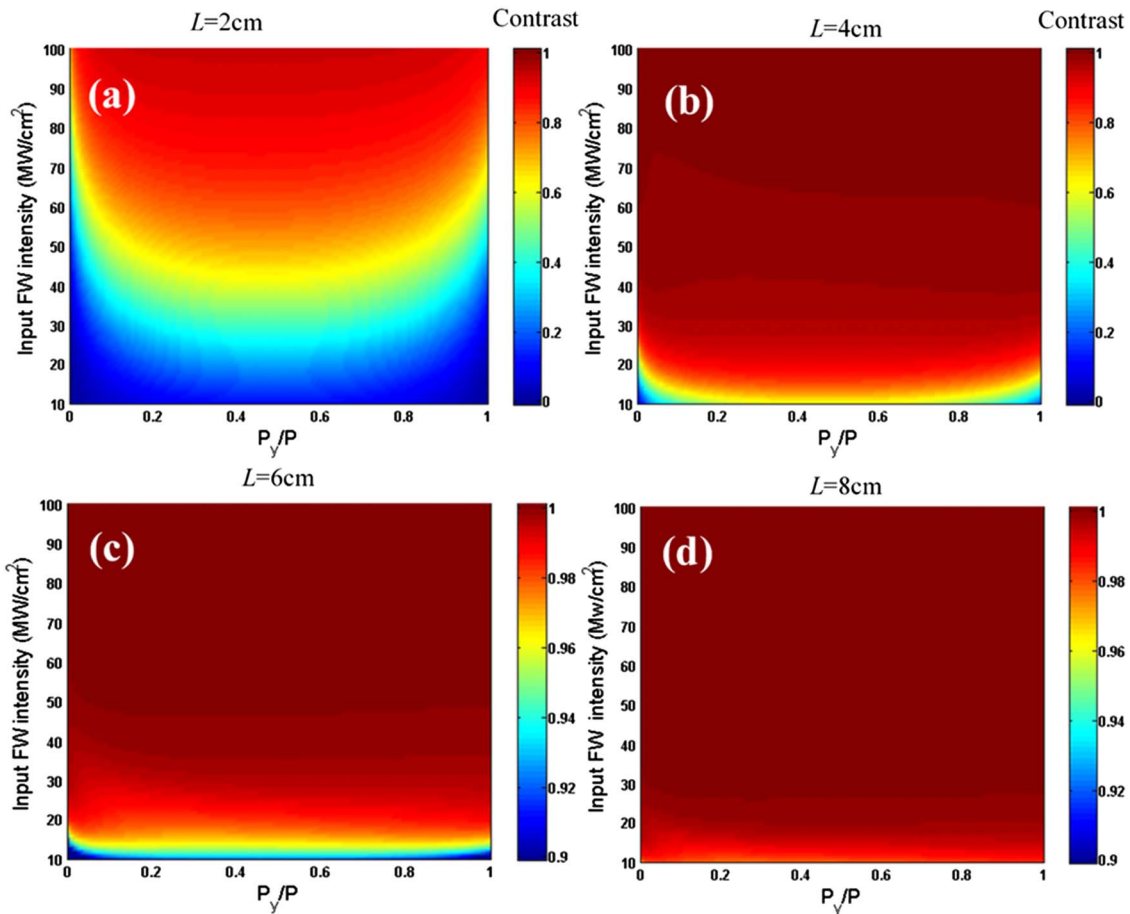

Fig. 7. (Color online) Contrast ratio versus the polarization state of the FW and the input intensity for different crystal lengths. (a) $L = 2\,\text{cm}$, (b) $L = 4\,\text{cm}$, (c) $L = 6\,\text{cm}$, and (d) $L = 8\,\text{cm}$. In these figures, $L_1/L = 0.1$ and $\delta L/\Lambda = 0.4$.

Low input intensity operation of the optical isolator is expected for a high contrast ratio under an arbitrary linearly polarization state. By numerical calculation, we find that increasing the whole length of the crystal while guaranteeing the defect in a strong asymmetry position at the same time is an effective way to achieve the goal. We set $L_1/L = 0.1$ and $\delta L/\Lambda = 0.2$ in our simulation. In Fig. 7(a), the crystal length is set at 2 cm. It shows that, only when the input FW intensity reaches as high as $100\,\text{MW/cm}^2$, can the contrast ratio maintain as 1 under the arbitrary linearly polarized light. When the length of the crystal increases to 4 cm, the optical diode can operate at $40\,\text{MW/cm}^2$ input intensity under an arbitrary linearly polarized FW, as shown in Fig. 7(b). However, under the current crystal growth technology, it is difficult to reach a PPLN length of more than 6 cm [22]. In theory, if the length of PPLN is 6 cm or even 8 cm, the required input intensity can be lowered to $20\,\text{MW/cm}^2$, or even lower than $10\,\text{MW/cm}^2$, which is shown in Figs. 7(c) and 7(d).

Our proposed theory to realize an all-optical optical isolator under arbitrary linearly polarized FW is available for both the continuous-wave and quasi-continuous-wave regimes. The pulsed regime has attracted interest in many applications, where the low-power tails of the pulse are unable to induce a significant nonlinear behavior. A detailed study of the pulsed regime, including considerations on the effects of nonzero mismatch in input and output segments, is far too complex and is outside the discussion in this paper.

4. Conclusion

In summary, we have proposed for the first time, to our knowledge, an all-optical isolator under an arbitrary linearly polarized input FW in an OSL. Our scheme is attractive in semiconductor laser diode systems because it can work without polarizers. Other advantages include that the period of the OSL can be designed at tens of micrometers and the defect length can be designed flexibly, which is convenient for fabricating a precise OSL to realize this type of all-optical isolator. In addition, a long OSL will realize an all-optical isolator for low optical intensities.

References

1. J. Fujita, M. Levy, R. M. Osgood, L. Wilkens, and H. Dotsch, "Waveguide optical isolator based on Mach–Zehnder interferometer," Appl. Phys. Lett. **76**, 2158–2160 (2000).
2. J. S. Yang, J. W. Roh, S. H. Ok, D. H. Woo, Y. T. Byun, W. Y. Lee, T. Mizumoto, and S. Lee, "An integrated optical waveguide isolator based on multimode interference by wafer direct bonding," IEEE Trans. Magn. **41**, 3520–3522 (2005).
3. T. Amemiya, H. Shimizu, M. Yokoyama, P. N. Hai, M. Tanaka, and Y. Nakano, "$1.54\,\mu\text{m}$ TM-mode waveguide optical isolator based on the nonreciprocal-loss phenomenon: device design to reduce insertion loss," Appl. Opt. **46**, 5784–5791 (2007).
4. E. Plum, V. A. Fedotov, and N. I. Zheludev, "Planar metamaterial with transmission and reflection that depend on the direction of incidence," Appl. Phys. Lett. **94**, 131901 (2009).
5. M. W. Feise, I. V. Shadrivov, and Yu. S. Kivshar, "Bistable isolator action in left-handed periodic structures," Phys. Rev. E **71**, 037602 (2005).
6. Z. F. Yu and S. H. Fan, "Complete optical isolation created by indirect interband photonic transitions," Nat. Photon. **3**, 91–94 (2009).
7. K. Gallo and G. Assanto, "All-optical isolator based on second-harmonic generation in an asymmetric waveguide," J. Opt. Soc. Am. B **16**, 267–269 (1999).
8. K. Gallo, G. Assanto, K. R. Parameswaran, and M. M. Fejer, "All-optical isolator in a periodically poled lithium niobate waveguide," Appl. Phys. Lett. **79**, 314–316 (2001).
9. Q. Wang, F. Xu, Z.-Y. Yu, X.-S. Qian, X.-K. Hu, Y.-Q. Lu, and H.-T. Wang, "A bidirectional tunable optical isolator based on periodically poled LiNbO_3," Opt. Express **18**, 7340–7346 (2010).
10. X.-S. Qian, H. Wu, Q. Wang, Z.-Y. Yu, F. Xu, Y.-Q. Lu, and Y.-F. Chen, "Electro-optic tunable optical isolator in periodically poled LiNbO_3," J. Appl. Phys. **109**, 053111 (2011).
11. Z.-Y. Yu, F. Xu, X.-W. Lin, X.-S. Song, X.-S., Qian, Q. Wang, and Y.-Q. Lu, "Tunable broadband isolator based on electro-optically induced linear gratings in a nonlinear photonic crystal," Opt. Lett. **35**, 3327–3329 (2010).
12. B. Johnston, P. Dekker, M. Withford, S. Saltiel, and Y. Kivshar, "Simultaneous phase matching and internal interference of two second-order nonlinear parametric processes," Opt. Express **14**, 11756–11765 (2006).
13. R. Lifshitz, A. Arie, and A. Bahabad, "Photonic quasicrystals for nonlinear optical frequency conversion," Phys. Rev. Lett. **95**, 133901 (2005).
14. Z. Liu, Y. Du, J. Liao, S. Zhu, Y. Zhu, Y. Qin, H. Wang, J. He, C. Zhang, and N. Ming, "Engineering of a dual-periodic optical superlattice used in a coupled optical parametric interaction," J. Opt. Soc. Am. B **19**, 1676–1684 (2002).
15. S. Zhu, Y. Zhu, and N. Ming, "Quasi-phase-matched third-harmonic generation in a quasi-periodic optical superlattice," Science **278**, 843–846 (1997).
16. K. Fradkin-Kashi, A. Arie, P. Urenski, and G. Rosenman, "Multiple nonlinear optical interactions with arbitrary wave vector differences," Phys. Rev. Lett. **88**, 023903 (2001).
17. G. K. Samanta, S. Chaitanya Kumar, M. Mathew, C. Canalias, V. Pasiskevicius, F. Laurell, and M. Ebrahim-Zadeh, "High-power, continuous-wave, second-harmonic generation at 532 nm in periodically poled KTiOPO_4," Opt. Lett. **33**, 2955–2957 (2008).
18. S. C. Kumar, G. K. Samanta, and M. Ebrahim-Zadeh, "High-power, single-frequency, continuous-wave second-harmonic-generation of ytterbium fiber laser in PPKTP and MgO: sPPLT," Opt. Express **17**, 13711–13726 (2009).
19. N. E. Yu, J. H. Ro, M. Cha, S. Kurimura, and T. Taira, "Broadband quasi-phase-matched second-harmonic generation in MgO-doped periodically poled LiNbO_3 at the communications band," Opt. Lett. **27**, 1046–1048 (2002).
20. J. Zhang, Y. Chen, F. Lu, and X. Chen, "Flexible wavelength conversion via cascaded second order nonlinearity using broadband SHG in MgO-doped PPLN," Opt. Express **16**, 6957–6962 (2008).
21. G. J. Edwards and M. Lawrence, "A temperature-dependent dispersion equation for congruently grown lithium niobate," Opt. Quantum Electron. **16**, 373–375 (1984).
22. I. Brener, M. H. Chou, D. Peale, and M. M. Fejer, "Cascaded $\chi^{(2)}$ wavelength converter in LiNbO_3 waveguides with counterpropagating beams," Electron. Lett. **35**, 1155–1157 (1999).